UDK 669.14:621.791
Original scientific article/Izvirni znanstveni članek

ISSN 1580-2949
MTAEC9, 58(4)477(2024)

COMPARATIVE STUDIES ON MICROSTRUCTURE AND TOUGHNESS OF 9 % Ni STEEL JOINTS WELDED BY SMAW AND GTAW

PRIMERJALNE ŠTUDIJE MIKROSTRUKTURE IN ŽILAVOSTI ZVARNIH SPOJEV MED PLOŠČAMA IZ MALO OGLJIČNEGA JEKLA Z 9 % Ni, IZDELANIMI Z SMAW IN GTAW

Haiyang Zhu[1,2], Xuebing Yang[3], Kun Liu[1], Xiaoyong Wang[4], Yuhang Du[1], Jiasheng Zou[1*]

[1]School of Materials Science and Engineering, Jiangsu University of Science and Technology, Zhenjiang, China
[2]School of Metallurgical Engineering, Suzhou Institute of Technology, Jiangsu University of Science and Technology, Suzhou, China
[3]Zhenjiang Zhongchuan Hitachi Zosen Machinery Co., Ltd., Zhenjiang, China
[4]School of Metallurgical Engineering, Jiangsu University of Science and Technology, Zhangjiagang, China

Prejem rokopisa – received: 2024-01-17; sprejem za objavo – accepted for publication: 2024-06-17

doi:10.17222/mit.2024.1096

The microstructure and impact toughness of 9 % Ni steel joints welded by shielded metal arc welding (SMAW) and gas tungsten arc welding (GTAW) were investigated. The two kinds of weld metal were mainly composed of cellular dendrites and a granular precipitated phase. The grains and cellular dendrites of the GTAW weld metal were smaller than those of the SMAW weld metal. The precipitates in the SMAW weld metal were stripe-shaped while those in the GTAW weld metal were rod-shaped; the number of precipitates in the GTAW weld metal was lower than in the SMAW weld metal. The low-temperature impact toughness of the GTAW weld metal was better than that of the SMAW weld melt.

Keywords: 9 % Ni steel, SMAW, GTAW, microstructure, impact toughness

Avtorji v članku opisujejo raziskavo mikrostrukture in udarne žilavosti zvarnih spojev plošč debeline 12 mm iz malo ogljičnega jekla z 9% Ni, ki so bili izdelani z obločnim varjenjem z oplaščeno kovinsko elektrodo (SMAW; angl.: shielded metal arc welding) in postopkom obločnega varjenja z volframovo elektrodo (GTAW; angl.: gas tungsten arc welding) v reaktivnem oziroma zaščitnem plinu. Med varjenjem sta nastali dve vrsti mikrostruktur v zvarnih spojih, ki sta v glavnem sestavljeni iz celične dendritne in granularne precipitatne faze. Kristalna zrna in celični dendriti GTAW zvarov so bili manjši kot tisti, ki so nastali med varjenjem s postopkom SMAW. Izločki (precipitati) v SMAW zvarih so imeli obliko trakov medtem, ko so imeli v GTAW zvarih obliko paličic. Število (koncentracija) izločkov v GTAW zvarih je bilo manjše od števila izločkov v SMAW zvarih. Nizko temperaturna udarna žilavost GTAW zvarov je bila boljša (višja) od žilavosti SMAW zvarov.

Ključne besede: jeklo z 9 % Ni, obločno varjenje z oplaščeno kovinsko elektrodo (SMAW), obločno varjenje z volframovo elektrodo (GTAW), zaščitna/reaktivna atmosfera, mikrostruktura, udarna žilavost

1 INTRODUCTION

Liquefied natural gas (LNG) as a clean and green energy fuel is gradually replacing coal and oil, leading to a rapid development of cryogenic storage-tank equipment.[1–3] Currently, 9 % Ni steel is the main material for manufacturing LNG cryogenic storage tanks. Compared with austenitic stainless steel and aluminum alloy, 9 % Ni steel has high strength, low thermal conductivity and thermal expansion coefficient, and good low-temperatures toughness.[4,5] In addition, good economic performance makes it an ideal material for cryogenic equipment.[6] In the market, 9 % Ni steel is commonly supplied in three states: double normalizing and tempering (NNT), quenching and tempering (QT), and two-phase region quenching and tempering (QLT).[7,8]

Welding is a necessary process for manufacturing LNG storage tanks. Welding consumables for 9 % Ni steel have been developed, transitioning from ferritic types to high nickel alloys. This change is attributed to the good fracture toughness of austenitic nickel-based alloy at low temperature.[9–11] Currently, the welding techniques for 9 % Ni steel include shielded metal arc welding (SMAW), submerged arc welding (SAW), gas metal arc welding (GMAW), gas tungsten arc welding (GTAW), flux cored arc welding (FCAW), laser beam welding (LBW), electron beam welding (EBW), etc.[12–18] Many scholars conducted comparative studies on 9 % Ni steel welded with different welding techniques. For example, Peng et al.[19] investigated the micro-segregation, microstructure, and bending properties of 9 % Ni steel weldments by SAW and SMAW. El-Batahgy et al.[20] studied the weldability of 9 % Ni steel using LBW and GTAW. Gook et al.[21] investigated the effect of welding parameters on the weld formation, microstructure and tensile strength of 9 % Ni steel welded in a single pass using three welding techniques: autogenous laser welding, laser cold wire welding and hybrid laser-arc weld-

*Corresponding author's e-mail:
zjzoujs@just.edu.cn (Jiasheng Zou)

Table 1: Compositions of the base metal and welding consumables (*w*/%)

Alloy	C	Si	Mn	P	S	Cr	Ni	Mo	Nb	Cu	Fe	W
9%Ni	0.05	0.27	0.66	0.005	0.002	0.03	9.12	0.002	–	0.01	–	–
ENiCrMo-6	0.03	0.31	2.73	0.005	0.01	12.36	66.37	5.82	1.12	0.05	5.70	1.39
ERNiCrMo-4	0.01	0.03	0.39	0.006	0.005	14.98	58.44	15.77	–	0.02	5.85	3.32

Table 2: Parameters of the two welding techniques

Technique	Current (A)	Voltage (V)	Speed (cm min^{-1})	Gas flow rate (l min^{-1})	Interlayer temperature (°C)	Heat input (kJ cm^{-1})
SMAW	130–140	24–28	12–16	–	< 100	14.7–15.6
GTAW	150–160	12–15	10–13	12	< 100	10.8–11.1

ing. The consumables for welding 9 % Ni steel commonly include Ni-Cr-Fe and Ni-Cr-Mo nickel-based alloys. The typical welding consumables for SMAW are ENiCrMo-3 and ENiCrMo-6 electrodes, while ERNiCrMo-3 and ERNiCrMo-4 wires are used for GTAW.[22] Huang[23] studied the microstructure and mechanical properties of joints welded by SMAW and GTAW using the ENiCrFe-9 and ERNiCrMo-4 filler metals, respectively. However, few comparative studies on 9 % Ni steel joints welded by SMAW and GTAW using the ENiCrMo-6 and ERNiCrMo-4 filler metals are found. For this study, two kinds of 9 % Ni steel joints were welded by SMAW and GTAW using welding electrode ENiCrMo-6 and welding wire ERNiCrMo-4, respectively. The differences in the microstructure and impact toughness of the two welded joints were investigated.

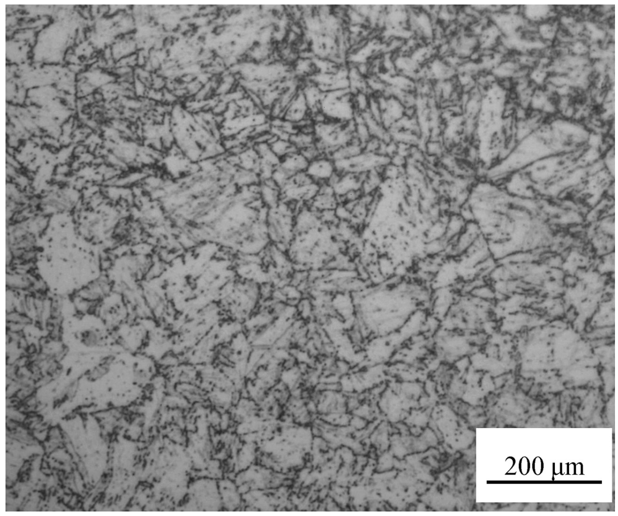

Figure 1: Microstructure of the base metal

2 EXPERIMENTAL PART

The base material was a 9 % Ni steel plate with the QT state and a thickness of 12 mm. **Figure 1** shows the optical microstructure of 9 % Ni steel with tempered martensite. Weld plates were produced by SMAW and GTAW. The welding consumables were an ENiCrMo-6 welding electrode for SMAW with a diameter of Φ 3.2 mm and an ERNiCrMo-4 welding wire for GTAW with a diameter of Φ 2.4 mm. The chemical compositions of the base metal and welding consumables are presented in **Table 1**.

The size of the welding plate was (300 × 240 × 12) mm, and the welding groove angle was 60°, as shown in **Figure 2**. A blunt edge of 2 mm was reserved for the SMAW plate, and a total of 5 layers and 8 passes were produced, with 3 layers on the front and 2 layers on the back. Single-sided welding with a double-sided forming process was used for the GTAW plate with a total of 6 layers and 10 passes. The welding parameters are shown in **Table 2**. The welding heat input was calculated using $Q = U \times I/S$, where Q, U, I and S represented the heat input, arc voltage, welding current, and welding speed, respectively. The heat input of SMAW was

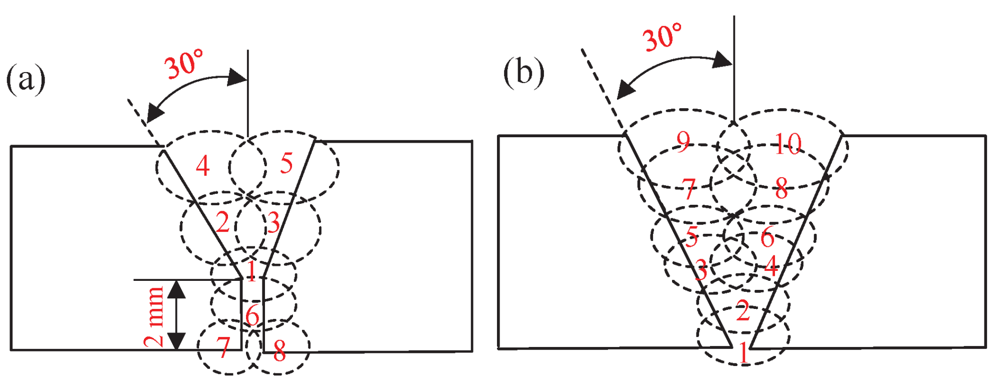

Figure 2: Schematic diagram of welding: a) SMAW, b) GTAW

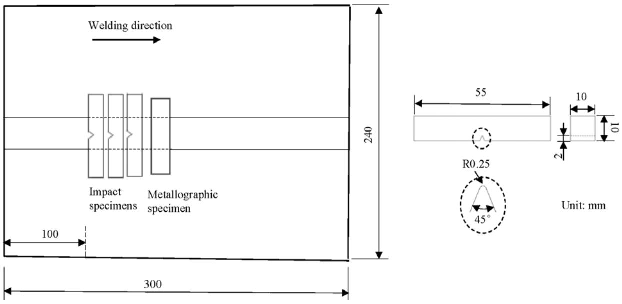

Figure 3: Position and dimensions of the impact specimen

14.7-15.6 kJ cm^{-1}, while the heat input of GTAW was 10.8–11.1 kJ cm^{-1}. The heat input of SMAW was about 4 kJ cm^{-1} higher than that of GTAW.

After the completion of welding, the microstructure and impact toughness were analyzed. The metallographic and impact samples were cut using a wire electrical discharge machine. After grinding and polishing, the weld zone of the metallographic sample was etched electrolytically in a 5 % chromic acid solution at a voltage of 4.5 V for 10 s, then the base metal was etched by a 4 % nitric alcohol solution. The metallographic microstructure was observed by a Zeiss Axio Imager A2m optical microscope (OM). The grain size of the weld metal was studied with Oxford C-Nano electron backscatter diffraction (EBSD). The EBSD specimens were firstly mechanically polished, then prepared with vibration polishing for 2–3 h using an Al_2O_3 agent. The precipitated phase was analyzed with a JSM-6510LA scanning electron microscope (SEM) and energy dispersive spectrometer (EDS). A V-notch impact test was carried out by a JB-300B pendulum impact testing machine at –196 °C. The position and dimensions of the impact sample are shown in **Figure 3**. The notch position was located at the cross-section of the weld zone. The fracture mechanism of the impact specimens was analyzed with SEM.

3 RESULTS AND DISCUSSION

3.1 Macrostructure and microstructure

The macrostructures of the welded joints obtained with SMAW and GTAW are shown in **Figures 4a** and **4b**. Macroscopic metallography showed that no defects such as crack, slag, incomplete penetration and incomplete fusion were present in the two welded joints. **Figures 4c** and **4d** show a cellular dendritic solidification mode that occurred in the SMAW and GTAW weld metal. It can be seen that the dendrite branches are of a bright color, while black particles exist among these dendrites, attributed to the residual liquid metal distributed between these branches during the crystallization process and the presence of a serious dendrite segregation.

Comparing the dendrite sizes and spacing types in the two weld metals, it was found that the GTAW den-

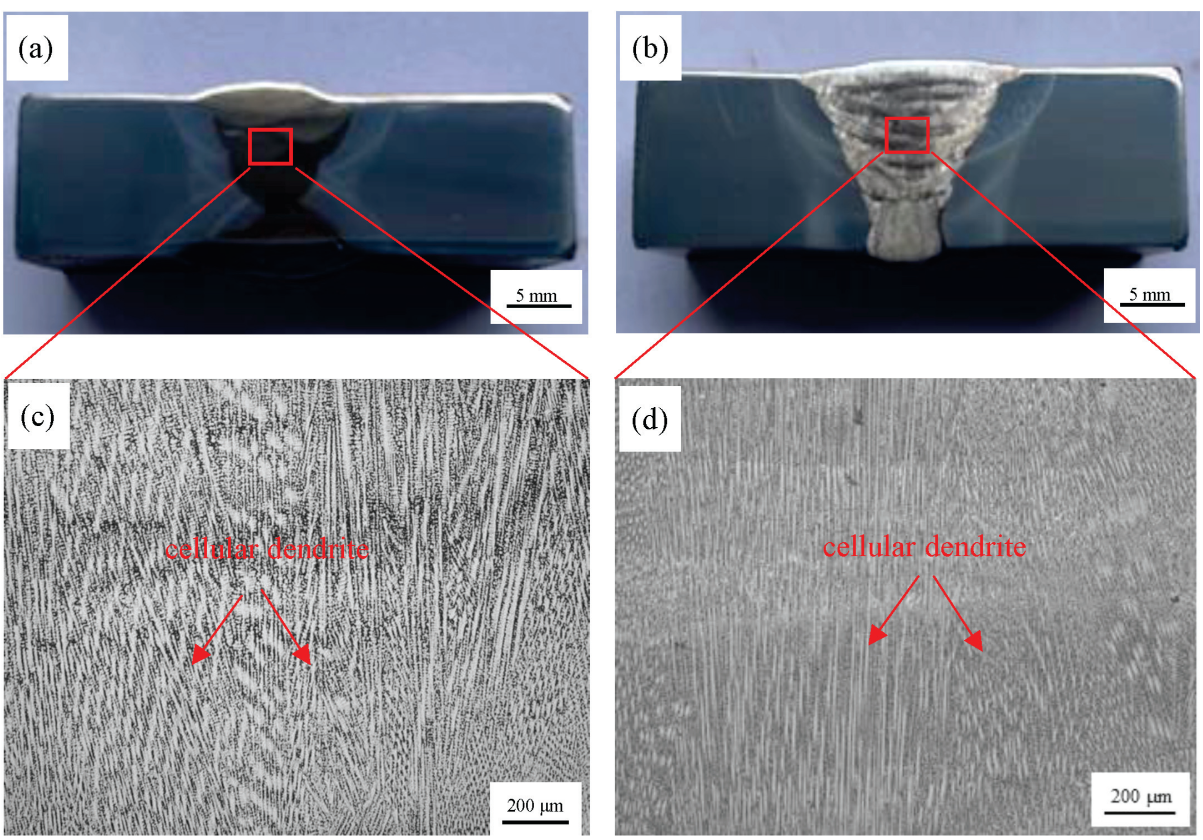

Figure 4: Macrostructure and microstructure of the weld metal: a), c) SMAW, b), d) GTAW

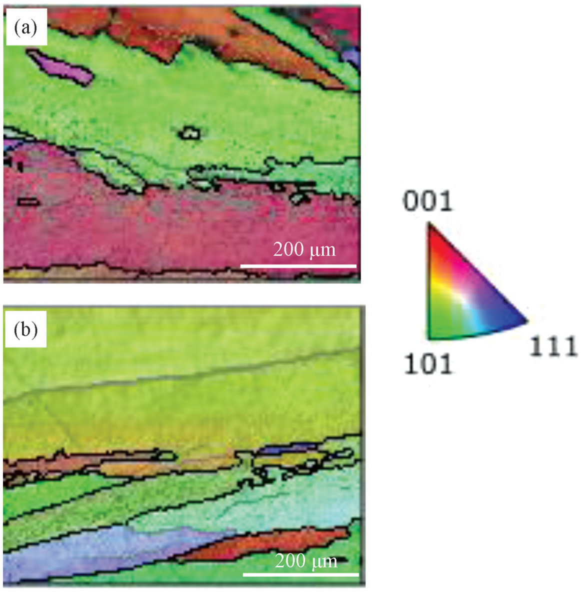

Figure 5: EBSD maps of the weld metal: a) SMAW, b) GTAW

drites were finer and the distance between adjacent dendrites was smaller than in the SMAW sample. To determine the grain size and grain orientation, EBSD was applied to each weld metal and the results are shown in **Figure 5**. Orientation maps were produced for the sections transverse to the welding direction. Inverse pole figures (IPF) showed that the width of grains in the SMAW weld metal was larger than in the GTAW weld metal.

The microstructures of the partially melted zone (PMZ) and heat affected zone (HAZ) of the two welded joints are shown in **Figures 6a** and **6c**. An obvious planar crystallization occurred in the PMZ, and the width of PMZ was a few tens of microns. Due to a higher heat input, more base-metal fusion occurred, and the width of the PMZ in the SMAW joint was larger than that in the GTAW joint. The crystal morphology was affected by temperature gradient *G* and crystallization rate *R*. At the bonding line, temperature gradient *G* was large and crystallization rate *R* was small; it was hard to induce constitutional supercooling, so a planar crystal was formed. With the solidification taking place from the bonding line to the center of the weld pool, temperature gradient G gradually decreased, while crystallization rate R gradually increased, and the constitutional supercooling zone gradually increased, so the crystal morphology changed from the planar crystal to cellular dendrite.[24]

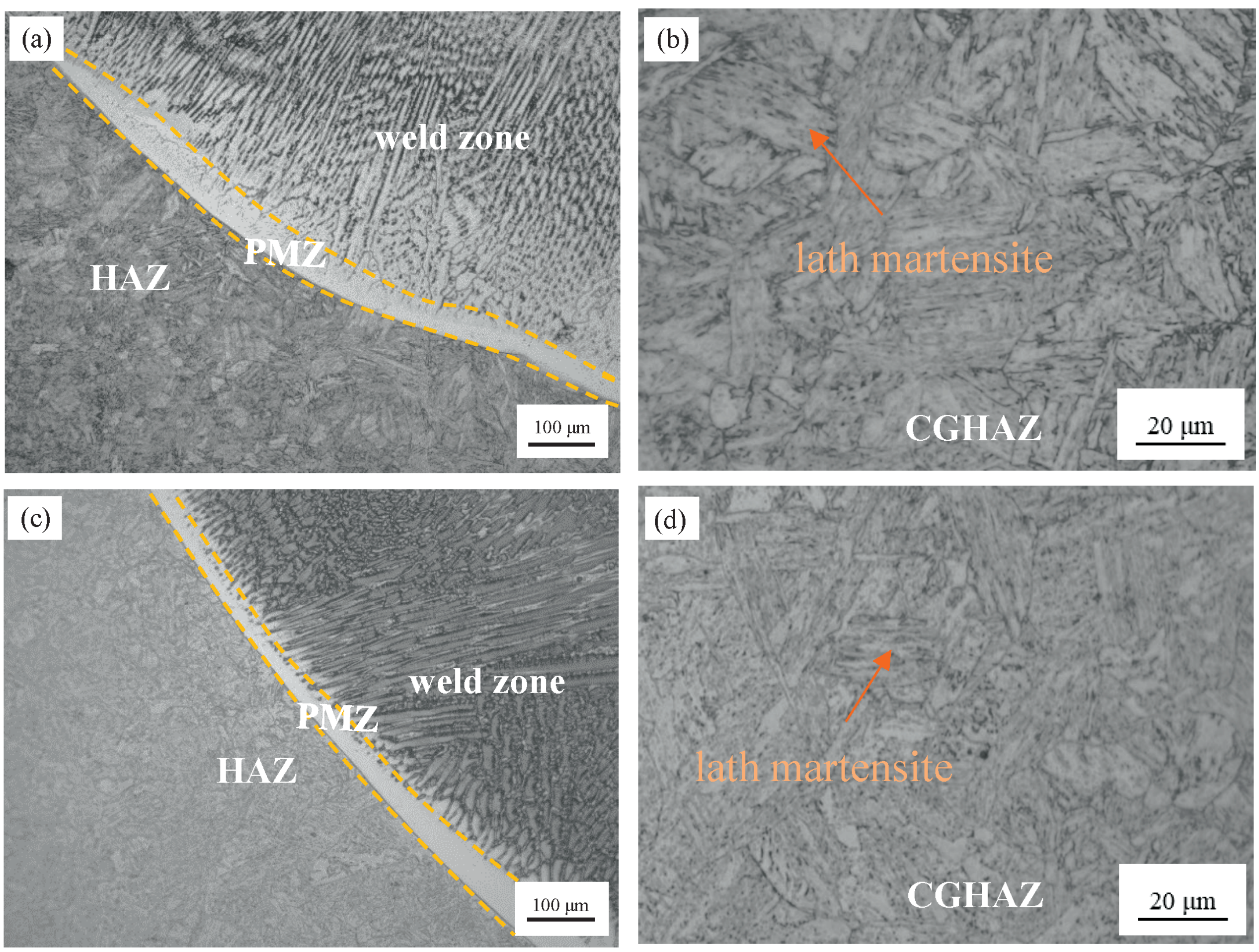

Figure 6: Microstructures of welded joints: a), b) SMAW, c), d) GTAW

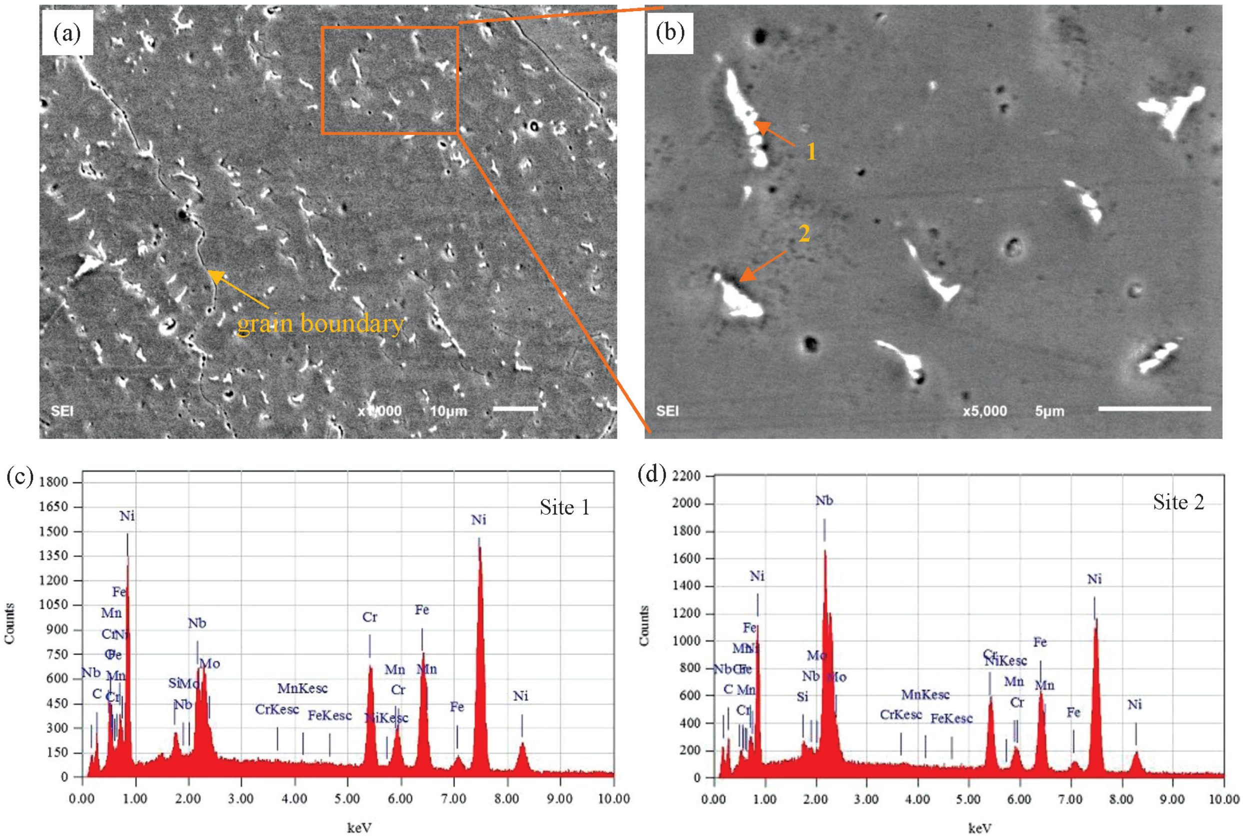

Figure 7: SEM images and EDS spectrums of SMAW weld metal: a), b) SEM images, c), d) EDS spectrums

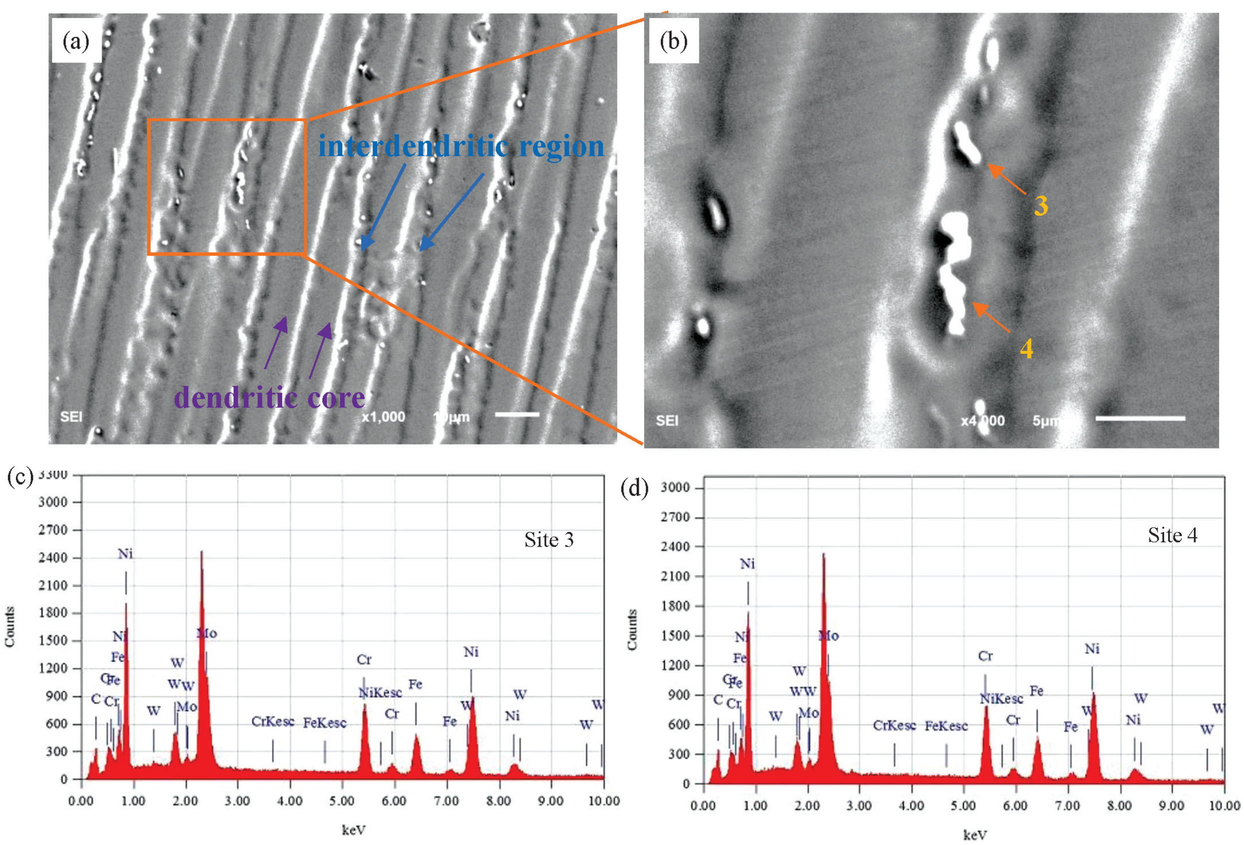

Figure 8: SEM images and EDS spectrums of GTAW weld metal: a), b) SEM images, c), d) EDS spectrums

Table 3: EDS results for the precipitated phases from **Figures 7b** and **8b** (*w*/%)

Weld metal	Sites	C	Si	Cr	Mn	Fe	Ni	Nb	Mo	W
SMAW	1	14.41	0.75	8.45	2.93	12.19	37.77	8.16	6.39	–
	2	16.85	0.53	7.97	1.91	11.17	35.38	10.14	6.76	–
GTAW	3	18.24	–	10.43	–	8.04	24.90	–	32.19	6.21
	4	18.81	–	10.50	–	7.86	25.97	–	31.82	5.04

Figures 6b and **6d** show the coarse grain HAZ (CGHAZ) of the two welded joints. Grains grew coarse due to rapid overheating and repeated thermal cycling. The higher heat input in the SMAW joint induced a longer time at high temperature, resulting in coarser lath martensite.

3.2 Precipitated phase

Figure 7a shows a SEM image of the SMAW weld metal. A large amount of precipitated phase is distributed in the matrix. The highly magnified image in **Figure 7b** shows that the intragranular precipitates formed discontinuous stripes with sharp ends. EDS analysis spectrums of these precipitates are presented in **Figures 7c** and **7d**, and the contents of elements are presented in **Table 3**. It can be seen that these precipitates are rich in Nb and Mo.

Figures 8a and **8b** show SEM images of the GTAW weld metal. It is obvious that these precipitates are distributed in interdendritic regions. Unlike the SMAW weld metal, the number of precipitates in this case is smaller, and the shape of precipitates mainly resembles rods with elliptical ends. This might be related to the chemical composition and cooling condition. The EDS results in **Figures 8c**, **8d** and **Table 3** show that the precipitates are rich in Mo and W.

The nickel-based welding electrode ENiCrMo-6 for SMAW contained a certain amount of Nb and Mo, while the nickel-based welding wire ERNiCrMo-4 for GTAW contained a certain amount of Mo and W (**Table 1**). These elements exhibit large atomic radius differences with Ni. For example, Mo and Nb, with their large atomic radii, tended to segregate in interdendritic regions, which resulted in a pronounced concentration gradient between dendritic and interdendritic regions, thus promoting the formation of (Nb, Mo)-rich and (Mo, W)-rich precipitates.[19,25,26]

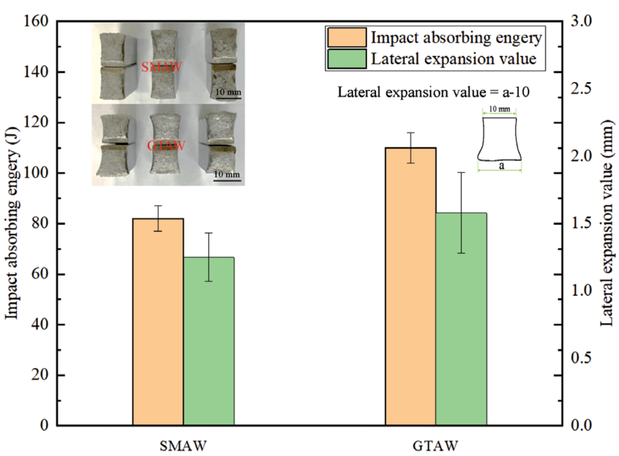

Figure 9: Impact absorbing energy and lateral expansion of SMAW and GTAW weld metal

3.3 Impact toughness

The results for the impact absorbing energy and lateral expansion at –196 °C for the two weld metals are shown in **Figure 9**. The average impact absorbing energy and lateral expansion values were used to characterize the impact toughness, where the lateral expansion referred to the sum of the maximum expansion on both sides of the specimen after impact fracture. When a specimen was subjected to a plane stress during the impact process, cracks were generated, and their propagation was squeezed outward, finally forming a lateral expansion. It can be seen that the average impact absorbing energy and lateral expansion of the SMAW weld metal are 82 J and 1.25 mm, respectively, while their values for the GTAW weld metal are 110 J and 1.58 mm, respectively. The impact absorbing energy of the GTAW weld metal is about 30 J higher than that for SMAW, and the lateral expansion of the GTAW weld metal is 26 % higher than that for SMAW. The results indicate that the low temperature toughness of the GTAW weld metal at –196 °C is better than for SMAW.

Figures 10a and **10d** show SEM images of the impact fractures of the SMAW and GTAW weld metal, respectively. The fracture surfaces were uneven and a large plastic deformation occurred. Highly magnified images of the fracture show two kinds of appearances: One includes dimples parallel to the length direction of cellular crystals, as shown in **Figures 10b** and **10f**, indicating that the width of cellular dendrite in the SMAW weld metal is significantly larger than that for GTAW. The other form includes equiaxed dimples and cleavage facets, as shown in **Figures 10c** and **10e**. The SMAW fracture exhibits a few dimples and some cleavage facets, while more dimples and fewer cleavage facets are observed in the GTAW weld metal. It can be inferred that the fracture was perpendicular to the length direction of cellular crystals. A higher impact toughness of the GTAW weld metal is attributed to the finer cellular dendritic crystals which increased the resistance to crack propagation. Moreover, the morphology and quantity of precipitates also influenced the toughness. As the SMAW weld metal had more precipitates with sharp ends than the GTAW weld metal, a high stress concentra-

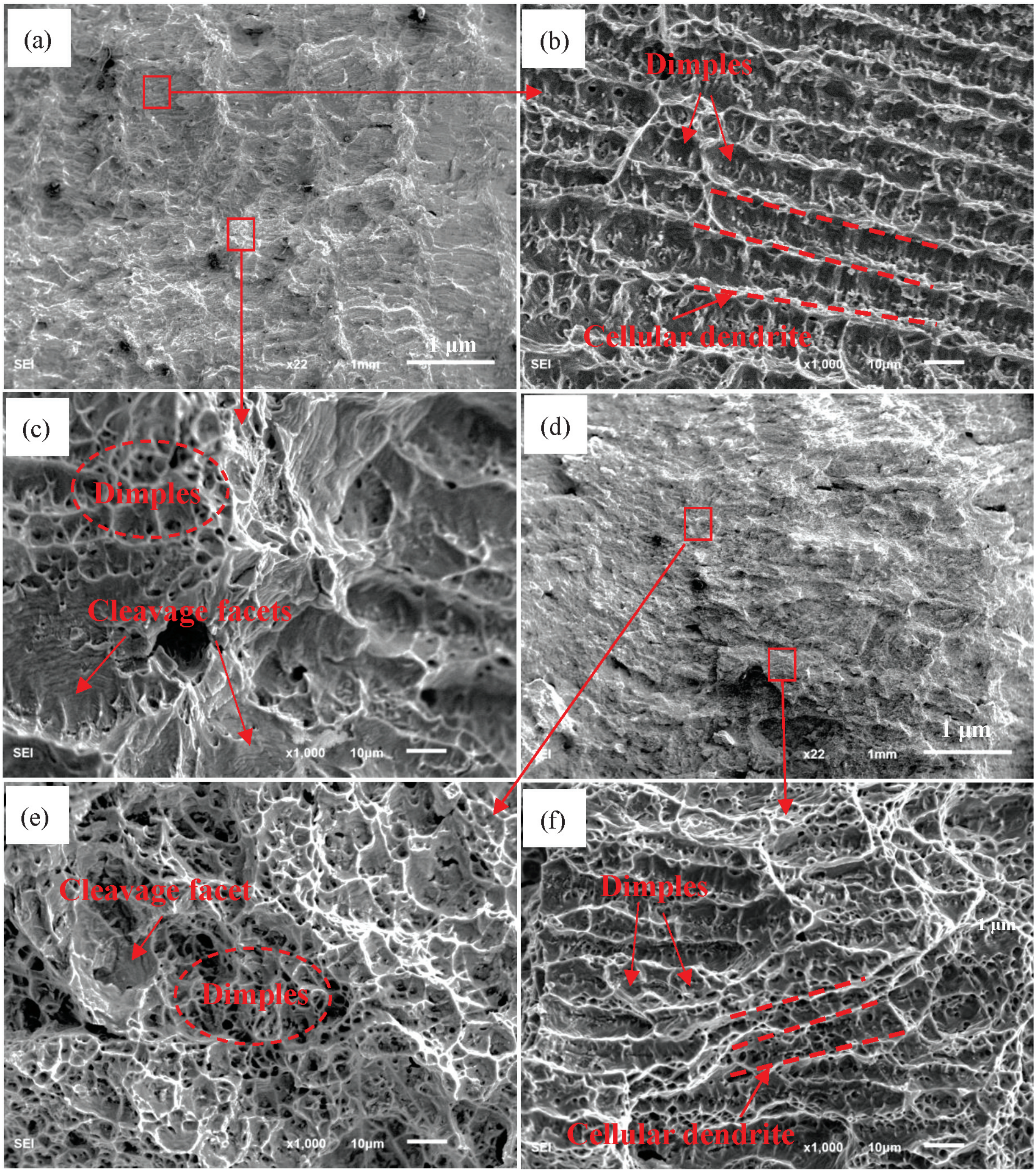

Figure 10: Fracture surfaces of impact specimens: a), b), c) SMAW; d), e), f) GTAW

tion and local plastic deformation occurred around these precipitates, which decreased the crack propagation resistance in the interdendritic region.[27]

4 CONCLUSIONS

The microstructure and impact toughness of 9 % Ni steel welded by SMAW and GTAW were studied. The main conclusions were as follows:

(1) The cellular dendrites of weld metal and the lath martensite of the CGHAZ in the GTAW joint were finer than those for SMAW, and the grain size of the GTAW weld metal was smaller.

(2) Precipitated phases were discontinuously distributed in the interdendritic region of weld metals. The precipitates in the SMAW weld metal mainly resembled stripes while rods were observed in the GTAW weld metal. The quantity of precipitates in the SMAW weld metal was higher than in the GTAW weld metal.

(3) The impact toughness of the GTAW weld metal at -196 °C was higher than for SMAW.

Acknowledgment

This work was supported by the National Natural Science Foundation of China (Grant No. 52105351), China Postdoctoral Science Foundation (Grant No. 2022M722928), Natural Science Foundation of Jiangsu Province (Grant No. BK20200997& BK20210890), and Jiangsu Provincial Double-Innovation Doctoral Program (Grant No. JSSCBS20210991).

5 REFERENCES

[1] J. Pospíšil, P. Charvát, O. Arsenyeva, L. Klimeš, M. Špiláček, J. J. Klemeš, Energy demand of liquefaction and regasification of natural gas and the potential of LNG for operative thermal energy storage, Renew. Sustain. Energy Rev., 99 (**2019**), 1–15, doi:10.1016/j.rser.2018.09.027

[2] D. J. Oh, J. M. Lee, B. J. Noh, W.S. Kim, Ryuichi-Ando, Toshiyuki-Matsumoto, M. H. Kim, Investigation of fatigue performance of low temperature alloys for liquefied natural gas storage tanks, Proc. Inst. Mech. Eng., Part C: J. Mech. Eng. Sci., 229 (**2015**) 7, 1300–1314, doi:10.1177/0954406215569255

[3] Y. Zhu, W. Mu, Y. Cai, D. Xin, M. Wang, A novel high-efficient welding technology with rotating arc assisted by laser and its application for cryogenic steels, J. Manuf. Process., 68 (**2021**), 1134–1146, doi:10.1016/j.jmapro.2021.06.042

[4] Y. Wu, Y. Cai, H. Wang, S. Shi, X. Hua, Y. Wu, Investigation on microstructure and properties of dissimilar joint between SA553 and SUS304 made by laser welding with filler wire, Mater. Des., 87 (**2015**), 567–578, doi:10.1016/j.matdes.2015.08.076

[5] S. Gook, S. Krieger, A. Gumenyuk, A. M. El-Batahgy, M. Rethmeier, Notch impact toughness of laser beam welded thick sheets of cryogenic nickel alloyed steel X8Ni9, Procedia CIRP, 94 (**2020**), 627–631, doi:10.1016/j.procir.2020.09.095

[6] K. Li, X. Wang, S. S. Rui, X. Li, S. Li, Q. Sun, Y. Zhang, Z. Cai, Fatigue crack growth mechanism of Ni-based weld metal in a 9 % Ni steel joint, Mater. Sci. Eng. A., 832 (**2022**), 142485, doi:10.1016/j.msea.2021.142485

[7] J. I. Jang, J. B. Ju, B. W. Lee, D. Kwon, W. S. Kim, Effects of microstructural change on fracture characteristics in coarse-grained heat-affected zones of QLT-processed 9 % Ni steel, Mater. Sci. Eng. A., 340 (**2003**) 1–2, 68–79, doi:10.1016/S0921-5093(02)00190-9

[8] J. I. Jang, J. B. Ju, B. W. Lee, D. Kwon, W. S. Kim, Micro-mechanism of local brittle zone phenomenon in weld heat-affected zones of advanced 9 % Ni steel, J. Mater. Sci. Lett., 20 (**2001**), 2149–2152, doi:10.1023/A:1013784600394

[9] A. El-Batahgy, A. Saiyah, S. Khafagi, A. Gumenyuk, S. Gook, M. Rethmeier, Shielded metal arc welding of 9 % Ni steel using matching ferritic filler metal, 26 (**2021**) 2, 116–122, doi:10.1080/13621718.2020.1846936

[10] A. Kern, U. Schriever, J. Stumpfe, Development of 9 % nickel steel for LNG applications, Steel Res. Int., 78 (**2007**) 3, 189–194, doi:10.1002/srin.200705879

[11] T. Xu, Y. Shi, Z. Jiang, B. Liu, J. Zhan, Z. Wang, An extraordinary improvement in cryogenic toughness of K-TIG welded 9Ni steel joint assisted by alternating axial magnetic field, J. Mater. Res. Technol., 25 (**2023**), 3071–3077, doi:10.1016/j.jmrt.2023.06.154

[12] M. Gustafsson, M. Thuvander, E. L. Bergqvist, E. Keehan, L. Karlsson, Effect of welding procedure on texture and strength of nickel based weld metal, Sci. Technol. Weld. Join., 12 (**2007**) 6, 549–555, doi:10.1179/174329307X213800

[13] R. Sakamoto, K. Kobayashi, T. Iijima, Y. Mizo, Development of submerged ARC welding method in a vertical upward position, Weld. World, 56 (**2012**), 64–71, doi:10.1007/BF03321366

[14] W. Guo, Y. Cai, B. Wang, B. Zhang, W. Mu, Effects of axial magnetic field on Fe-Ni interface macrosegregation of 9 %Ni steel welds filled with Ni-based alloy, J. Mater. Process. Technol., 315 (**2023**), 117889, doi:10.1016/j.jmatprotec.2023.117889

[15] H. T. Serindağ, C. Tardu, İ. Ö. Kirçiçek, G. Çam, A study on microstructural and mechanical properties of gas tungsten arc welded thick cryogenic 9 % Ni alloy steel butt joint, CIRP J. Manuf. Sci. Technol., 37 (**2022**), 1–10, doi:10.1016/j.cirpj.2021.12.006

[16] W. Mu, Y. Li, Y. Cai, M. Wang, Cryogenic fracture toughness of 9%Ni steel flux cored arc welds, J. Mater. Process. Technol., 252 (**2018**), 804–812, do:10.1016/j.jmatprotec.2017.10.026

[17] Y. Wu, Y. Cai, D. Sun, J. Zhu, Y. Wu, Microstructure and properties of high-power laser welding of SUS304 to SA553 for cryogenic applications, J. Mater. Process. Technol., 225 (**2015**), 56–66, doi:10.1016/j.jmatprotec.2015.05.011

[18] J. Grandgirard, D. Poinsot, L. Krespi, J. P. Nénon, A. M. Cortesero, Weld metal impact toughness of electron beam welded 9 % Ni steel, Entomol. Exp. Appl., 36 (**2001**), 1197–1200, doi:10.1023/A:1004890027527

[19] H. Peng, X. Liu, C. Deng, S. Wu, Q. Li, L. Ma, Evolution of microsegregation-induced precipitations and bending fracture mechanisms of 9 % Ni steel weldments filled with nickel-based alloys, J. Mater. Res. Technol., 26 (**2023**), 42–57, doi:10.1016/j.jmrt.2023.07.178

[20] A. M. El-Batahgy, A. Gumenyuk, S. Gook, M. Rethmeier, Comparison between GTA and laser beam welding of 9 %Ni steel for critical cryogenic applications, J. Mater. Process. Technol., 261 (**2018**), 193–201, doi:10.1016/j.jmatprotec.2018.05.023

[21] S. Gook, M. Forquer, A. M. El-Batahgy, A. Gumenyuk, Laser and hybrid laser-arc welding of cryogenic 9 % Ni steel for construction of LNG storage tanks, Proc. of the 3rd Inter. Conf. Africa and Asia on Welding and Failure Analysis of Engineering Materials, Luxor 2015, 2–5

[22] J. Hilkes, F. Neessen, Welding 9 % nickel steel for liquefied natural gas (LNG) applications, Weld. Cut., 6 (**2007**), 103–112

[23] J. X. Huang, The Double-sided Synchronous TIG Procedure and Matching Analysis of Corresponding Joint of X7Ni9 Steel, Procedia Eng., 130 (**2015**), 517–523, doi:10.1016/j.proeng.2015.12.256

[24] S. Kou, Welding Metallurgy, 2nd ed., John Wiley & Sons, New Jersey, 2002, 158–159

[25] Z. Qiu, B. Wu, H. Zhu, Z. Wang, A. Hellier, Y. Ma, H. Li, O. Muransky, D. Wexler, Microstructure and mechanical properties of wire arc additively manufactured Hastelloy C276 alloy, Mater. Des., 195 (**2020**), 109007, doi:10.1016/j.matdes.2020.109007

[26] W. Wang, L. Jiang, C. Li, B. Leng, X. X. Ye, R. Liu, S. Chen, K. Yu, Z. Li, X. Zhou, Effects of post-weld heat treatment on microstructure and mechanical properties of Hastelloy N superalloy welds, Mater. Today Commun., 19 (**2019**), 230–237, doi:10.1016/j.mtcomm.2019.02.004

[27] W. Mu, Y. Cai, M. Wang, Effect of precipitates on the cryogenic fracture toughness of 9 % Ni steel flux cored arc weld, Mater. Sci. Eng. A., 819 (**2021**), 141418, doi:10.1016/j.msea.2021.141418